J. Phys. B: At. Mol. Opt. Phys. 26 (1993) 1445–1461. Printed in the UK

Harmonic generation in ionizing systems by the time-dependent complex coordinate Floquet method

Nir Ben-Tal†, Nimrod Moiseyev†, Ronnie Kosloff‡ and Charles Cerjan§

† Department of Chemistry, Technion–Israel Institute of Technology, Haifa 32000, Israel
‡ The Fritz Haber Research Center for Molecular Dynamics, The Hebrew University, Jerusalem 91904, Israel
§ Lawrence Livermore National Laboratory, Livermore, CA 94550, USA

Received 12 November 1992

Abstract. The time-dependent complex coordinate Floquet method was developed for the study of non-linear phenomena observed for atoms (or small molecules) in strong laser fields. On the basis of this method and by taking use of the special definition of the inner product for non-Hermitian operators a simple time-independent expression for the probability to obtain high harmonics was derived. This novel formula is used to investigate the phenomenon of harmonic generation for a model potential representing a single electron in the presence of an intense laser field. The parameters of the one-dimensional potential are chosen to fit two electronic states of the xenon atom. Numerical results indicate the existence of a correlation between harmonic generation and other non-linear effects occurring in this system such as avoided crossings of Floquet resonance states as the field strength amplitude is varied. The harmonic generation spectra obtained by the model presented here qualitatively agree with experimental results on rare gas atoms placed in strong laser fields. For strong laser fields ($> 10^{14}$ W cm^{-2}), very-high-order harmonic generation is observed in numerical studies using both complex Floquet analysis and a simulation by a pseudo-spectral grid solution to the time-dependent Schrödinger equation with a non-periodic Hamiltonian. For *extremely* strong laser fields, numerical results predict that the most intense frequency emitted by an atom interacting with a monochromatic laser field might not be the irradiating laser frequency, but rather a high multiple of it.

1. Introduction

Recently, experiments monitoring the spectrum emitted from strongly irradiated low pressure rare-gas atoms were carried out [1, 2]. Spectra obtained in these experiments were found to consist of the fundamental frequency of the irradiating laser field, and high harmonics of this frequency. This phenomenon, that is by no means a new one, is often called harmonic generation, HG. In typical harmonic generation experiments involving rare-gas atoms, only odd multiples of the original frequency are produced. This phenomenon was attributed to the fact that parity is a good quantum number in gaseous systems. A characteristic HG spectrum exhibits an exponential decay of the intensity of first few (about three) peaks relative to the intensity of the fundamental frequency. This decay is followed by a plateau approximately between the 5th and the 25th harmonics. The plateau ends in an exponential decay. Smaller sub-harmonic peaks are often detected as well. These sub-harmonics have been attributed to the interaction of resonance states [3].

The existence of a plateau in the HG spectrum requires a constant phase-matching factor for all harmonics (roughly speaking, the phase-matching factor describes the interaction of

0953-4075/93/081445+17$07.50

radiation coming from different irradiated gas atoms acting as secondary radiation sources). Indeed, L'Huillier *et al* have found in a theoretical study that, unlike the case in low intensity fields, for high intensity fields the phase matching factor is almost constant for all harmonic orders [4]. The constancy of phase matching ensures that the high-order harmonics will indeed propagate out of the experimental interaction region and hence be observable.

The appearance of a plateau which extends to high harmonics raised the hope of multiplying the UV laser frequency by a factor of about 100 to reach the soft x-ray regime, so that an efficient laboratory source of coherent x-ray radiation would be feasible. Producing such a source in an efficient manner requires an HG spectrum consisting of a *single* harmonic peak at a frequency of about 100 times that of the incoming UV laser frequency. It is hoped that harmonic generation will provide an opportunity for producing small and portable equipment which will be able to multiply the (already existing) UV laser frequency to the x-ray regime. Such an apparatus might have a variety of applications such as: production and investigation of fusion plasmas, creation of holograms of microscopic biological structures (proteins, hierarchical twistings that transform the DNA from its basic double helix structure into the compact structure of chromosomes, etc.) and solid surface characterization, to mention just a few proposed applications [6]. Existing coherent x-ray sources, such as x-ray lasers [7], require large laser facilities and are relatively inefficient.

The possible applications of coherent x-ray sources have encouraged classical [8], semiclassical [6, 9, 12–15] and quantum [3, 11] theoretical studies in order to understand the mechanism underlying efficient high-order harmonic generation for possible future optimization. It was shown by Kulander [16], and later on in detail by Eberly *et al* [12] and by Pan *et al* [17] that the experiments were carried out in field strengths ($\sim 10^{14}$ W cm^{-2}) which are beyond the applicability of a simple perturbative treatment. Some non-perturbative methods have already been used to calculate the HG spectrum [3, 6, 8–17]. Szöke [15] has developed a quantum-mechanical, many-body theory of multiphoton excitation using a two-time expansion technique, a Floquet basis set and a complex rotation of the coordinates. The central goal of his theory was to include as much of the motion of bound and free electrons as convenient into non-perturbative formulae and to do perturbation theory on the rest. Kulander and co-workers [9] have used a time-dependent mean field method to treat some irradiated rare-gas atom systems. Their main conclusion has been that not only is the process governed by a *single atom*, but also by a *single electron*. Eberly and co-workers [12] have shown in their one-dimensional calculations a connection between the HG phenomenon and another non-linear phenomenon—above threshold ionization, ATI, (the discovery that in high laser fields ionized photoelectrons are emitted at energies which are greater than the ionization potential by integer multiples of the field frequency) and demonstrated both phenomena in a model calculation. Potvliege and Shakeshaft have studied many examples of multiphoton processes (including the HG and ATI phenomena) for a hydrogen atom [13]. Bardsley *et al* [18] have shown numerically that ATI spectra can be understood by a model which takes into account only the interaction of a single bound electron with an external *periodic* laser field (i.e. neglecting the envelope of the laser pulse). The success of Potvliege and Shakeshaft [13] to use the Floquet ansatz in calculating a HG spectrum of the hydrogen atom which agrees with experimental observations is consistant with these findings. In this paper we proceed along these lines to study the HG phenomena by a one-dimensional model interacting with a monochromatic intense radiation field.

An alternative theoretical approach for time periodic system is the time-dependent complex coordinate Floquet method, TDCCFM. In the next section we describe this method. In section 3 we derive an expression for calculating the HG spectrum by this method. In

section 5 we present and discuss numerical results; section 6 summarizes and concludes this work.

2. The time-dependent complex coordinate Floquet method

The time-dependent complex Floquet method, TDCCFM, is a non-perturbative semiclassical approach (that is, the external field is described classically). This method is applicable for exploring linear and non-linear phenomena caused by interaction of a time periodic field with an atom or a molecule. The method has been used for the study of positions, lifetimes and partial widths of metastable quasi-energy states [19], as well as for the study of creation and annihilation of metastable quasi-energy states in strong laser fields [20]. The method has been described in detail in a previous article [19]. Here we shall outline the main points.

Conservative systems, which have energy as a good quantum number, do not retain this convenient property when coupled to an external time-dependent field. In the case of a *time periodic* external field, however, the Floquet theorem [21] suggests an alternative good quantum number—the *quasi-energy*. This theorem states that a solution of the time-dependent Schrödinger equation (using atomic units)

$$\mathrm{i}\frac{\partial\psi_\alpha(\boldsymbol{x},\,t)}{\partial t}=\hat{H}(\boldsymbol{x},\,t)\psi_\alpha(\boldsymbol{x},\,t) \tag{2.1}$$

where $\hat{H}(\boldsymbol{x},\,t)$ is a time periodic Hamiltonian operator with a period of $T=2\pi/\omega$,

$$\hat{H}(\boldsymbol{x},\,t)=\hat{H}(\boldsymbol{x},\,t+nT)\qquad n=0,\pm1,\pm2,\ldots \tag{2.2}$$

has the form

$$\psi_\alpha(\boldsymbol{x},\,t)=\mathrm{e}^{-\mathrm{i}\varepsilon_\alpha t}\Phi_\alpha(\boldsymbol{x},\,t) \tag{2.3}$$

where

$$\Phi_\alpha(\boldsymbol{x},\,t)=\Phi_\alpha(\boldsymbol{x},\,t+nT). \tag{2.4}$$

Consequently, $\Phi_\alpha(\boldsymbol{x},\,t)$ is a time periodic function termed a Floquet state or quasi-energy state, with the associated quasi-energy, ε_α.

For a dissociative (ionizing) system, that supports a few bound states, the interaction with the external periodic field might turn the bound states into states with finite lifetimes. As a result they become *resonance* states. A complex rotation of the coordinates $\boldsymbol{x}$ appearing in the Hamiltonian by an angle θ into the complex plane (i.e. $\boldsymbol{x}\rightarrow\mathrm{e}^{\mathrm{i}\theta}\boldsymbol{x}$), makes it possible to describe each resonance state by a single square integrable wavefunction. Furthermore, following the Balslev and Combes theorem [22], the resonance states become distinguishable from the continuum [23].

The complex scaled time evolution operator $\hat{U}_\theta(t|0)$ is defined [24] by

$$\psi_\alpha\left(\mathrm{e}^{\mathrm{i}\theta}\boldsymbol{x},\,t\right)=\hat{U}_\theta(t|0)\psi_\alpha\left(\mathrm{e}^{\mathrm{i}\theta}\boldsymbol{x},\,0\right). \tag{2.5}$$

Substituting equations (2.3) and (2.4) in (2.5) for $t=T$, one obtains the complex eigenvalue equation

$$\hat{U}_\theta(T|0)\phi_\alpha\left(\mathrm{e}^{\mathrm{i}\theta}\boldsymbol{x},\,0\right)=\lambda_\alpha\Phi_\alpha\left(\mathrm{e}^{\mathrm{i}\theta}\boldsymbol{x},\,0\right) \tag{2.6}$$

where

$$\lambda_\alpha = e^{-i\tilde{\varepsilon}_\alpha T} \tag{2.7}$$

and $\tilde{\varepsilon}_\alpha$ is a complex quasi-energy. The quasi-energy $\tilde{\varepsilon}_\alpha$ might be associated with a resonance state $|\phi_\alpha\rangle$ in which case it is (in principle) θ-independent with $\tilde{\varepsilon}_\alpha = \varepsilon_\alpha - i\Gamma_\alpha/2$. Here, ε_α is the energy position and $\Gamma_\alpha = \hbar/\tau_\alpha$ is the energy width that is inversely proportional to the lifetime τ_α of the resonance state $|\phi_\alpha\rangle$. In cases where $|\Phi_\alpha\rangle$ is associated with a continuum state $\tilde{\varepsilon}_\alpha = \varepsilon_\alpha e^{-2i\theta}$ so that the value is explicitly θ dependent. From equation (2.7) it is clear that the (θ-dependent) continuum states form a spiral that converges to the origin (0,0) in the complex λ plane. The (θ-independent) resonance states on the other hand, are located outside this spiral, on the unit circle or inside it. The distance of a resonance state from the origin (0, 0) is a measure of its lifetime τ_α. A bound state with an infinite lifetime (zero width) will be located on the unit circle, whereas a resonance state, having a shorter lifetime (broad width) will appear closer to the origin (0,0). The angle with the horizontal axis is a measure of the resonance position ε_α modulus $\hbar\omega$. Figure 1(a) represents the λ complex plane obtained by the model Hamiltonian described in section 4 for a specific choice of parameters. The resonance states are clearly separated from each other and from the spiral associated with the continuum.

A computational procedure (the TDCCFM) for obtaining resonance states is thus based on equations (2.5) and (2.6). First, solve the evolution equation to obtain the complex scaled time evolution matrix $\mathbf{U}_\theta(T|0)$ for the normalized initial conditions $\hat{\mathbf{U}}_\theta(0|0) = \mathbf{I}$ (where $\mathbf{I}$ is a unit matrix)

$$i\frac{d\mathbf{U}_\theta(t|0)}{dt} = \mathbf{H}_\theta(t)\mathbf{U}_\theta(t|0) \tag{2.8}$$

with the (known) complex scaled time periodic Hamiltonian matrix $[\mathbf{H}_\theta(t)]_{i,j} = \langle i|\hat{H}(xe^{i\theta}, t)|j\rangle$. Second, diagonalize the time evolution matrix $\mathbf{U}_\theta(T|0)$ to find the matrix analogue of equation (2.6): the Floquet quasi-energy eigenvectors and the corresponding eigenvalues λ_α. Finally, by plotting $\mathrm{Re}(\lambda_\alpha)$ against $\mathrm{Im}(\lambda_\alpha)$ (as shown in figure 1(a)) one can distinguish between the θ-independent isolated resonance states and the θ-dependent continuum states.

Solving the Schrödinger equation (2.8) requires a representation of the Hamiltonian as a matrix in some basis set. Propagation of $\mathbf{U}_\theta(t|0)$ according to equation (2.8) can be done by several algorithms. Several possible representations and algorithms are compared elsewhere [19]. In the present work we used a Fourier basis set for the representation of the Hamiltonian. Solution of equation (2.8) was carried out in the integrated form, where the evolution matrix was evaluated at small time steps, Δt, for which the Hamiltonian was assumed to be almost constant. The time-ordered expression, $\hat{T}\exp[-i\int \hat{H}(t)dt]$, where $\hat{T}$ is the time ordering operator, was approximated by a second-order Magnus series. Matrix exponentiation was carried out by a Taylor expansion of 5th to 10th order. The operation of the Hamiltonian on the time evolution matrix $U(t|0)$ was carried out for the kinetic part and for the potential part separately. Forward and backward fast Fourier transforms were used for transforming the evolution matrix from momentum space to configuration space and vice versa [25–28].

The main advantage of the TDCCFM is the ability to describe a resonance state by a single square integrable, L^2, function. Representation of the quasi-energy states in the complex λ plane enables us to study the dependence of the resonance positions and widths on the field frequency and intensity. In the λ plane representation it is easy to monitor interactions between close resonances that go through avoided crossings as field parameters are changed.

3. Harmonic generation spectra by the time-dependent complex coordinate Floquet method

The complex scaled quasi-energy resonance states $\Phi_\alpha(e^{i\theta}\boldsymbol{x}, 0)$ and the eigenvalues, λ_α, obtained by diagonalization of the one optical cycle time evolution matrix, provide the basis for understanding many non-linear phenomena. In this section we shall demonstrate how these quantities can be used for calculating the harmonic response spectrum.

Let $\psi(e^{i\theta}\boldsymbol{x}, t)$ denote the state of a particular system at a given time (for example, a rare-gas atom in the presence of a laser field). Since the Floquet quasi-energy states $\Phi_\alpha(e^{i\theta}\boldsymbol{x}, t)$ form a complete set, they can be used as basis functions such that

$$\psi(e^{i\theta}\boldsymbol{x}, t) = \sum_\alpha c_\alpha e^{-i\tilde{\varepsilon}_\alpha t}\Phi_\alpha(e^{i\theta}\boldsymbol{x}, t) \tag{3.1}$$

with time-independent coefficients c_α. For large enough scaling angle θ, the continuum will not contribute much to the sum in equation (3.1), therefore we may restrict the sum in equation (3.1) to a sum over only the resonance states

$$\psi(e^{i\theta}\boldsymbol{x}, t) \simeq \sum_{\substack{\alpha \\ \text{resonance}}} c_\alpha e^{-i\tilde{\varepsilon}_\alpha t}\Phi_\alpha(e^{i\theta}\boldsymbol{x}, t). \tag{3.2}$$

Usually there is a single isolated resonance state with a relatively large lifetime, that is, a small value of $\mathrm{Im}(\tilde{\varepsilon}_\alpha)$. In such a case, the contributions of all other resonance states to the sum are negligible compared to the contribution of this state. Very frequently we can replace the sum in equation (3.2) by the *resonance state which has the largest lifetime*, $\Phi_{\mathrm{res}}, (e^{i\theta}\boldsymbol{x}, t)$ for which $\mathrm{Im}(\tilde{\varepsilon}_\alpha)$ gets a minimal value. That is,

$$\psi(e^{i\theta}\boldsymbol{x}, t) \simeq e^{-i\tilde{\varepsilon}_{\mathrm{res}}t}\Phi_{\mathrm{res}}(e^{i\theta}\boldsymbol{x}, t). \tag{3.3}$$

One can see from equation (3.3) that, under the above mentioned conditions, the dynamics of the system in the long time limit is governed by the single narrowest (largest lifetime) resonance state.

In the dipole approximation using the radiation gauge, the HG spectrum $\sigma(\Omega)$ is defined as the set of frequencies which construct the expectation value of the momentum operator

$$\sigma(\Omega) \propto \left|\frac{1}{T}\int_0^T e^{-i\Omega t} D(t)\mathrm{d}t\right|^2 \tag{3.4}$$

where

$$D(t) = \langle\langle\psi_{\mathrm{res}}(\theta, t)\big|\hat{p}\big|\psi_{\mathrm{res}}(\theta, t)\rangle\rangle \tag{3.5}$$

is calculated for one optical cycle. The notation $\langle\langle\ldots\ldots\rangle\rangle$ stands for a complex inner product—no complex conjugation of terms which are complex as a result of scaling [29]. This definition of the inner product is fundamental in the theory of analytic continuation and enables the calculation of the harmonic response regardless of the magnitude of $\mathrm{Im}(\tilde{\varepsilon})$.

A simple way to calculate the expectation value of $\hat{p}$ in equation (3.5) is by expanding the periodic part $\Phi_{res}(e^{i\theta}x, t)$ of equation (3.3) in a Fourier series

$$\Phi_{res}(e^{i\theta}x, t) = \sum_{k=-\infty}^{\infty} \phi_k^{res}(e^{i\theta}x)e^{i\omega kt}. \tag{3.6}$$

Substituting equation (3.6) into (3.4) with the use of equation (3.5) and equation (3.3); then making explicit use of the orthonormality of $\phi_k^{res}(e^{i\theta}x)$ leads to the following equation for the probability of obtaining frequency Ω

$$\sigma(\Omega = n\omega) \propto \left| \sum_{k=-\infty}^{\infty} \langle\langle \phi_{k+n}^{res}(\theta) | \hat{p} | \phi_k^{res}(\theta) \rangle\rangle \right|^2. \tag{3.7}$$

As a summary, we outline here the proposed procedure.

(i) The TDCCFM (as outlined in section 2) is used to obtain the resonance state which has the largest lifetime $\Phi_{res}(e^{i\theta}x, 0) = e^{i\tilde{\varepsilon}_{res}T}\psi_{res}(e^{i\theta}x, T)$.

(ii) $\Phi_{res}(e^{i\theta}x, 0)$ is propagated to obtain $\Phi_{res}(e^{i\theta}x, t)$ for $0 \leqslant t < T$. The Fourier components, $\phi_k^{res}(e^{i\theta}x)$, of the resonance function (defined in equation (3.6)) are calculated.

(iii) $\sigma(\Omega = n\omega)$ is calculated by using the Fourier components $\phi_k^{res}(e^{i\theta}x)$ (in the frequency domain) using equation (3.7).

4. Model and methods

4.1. The time-dependent complex coordinate Floquet theory

In the framework of the semiclassical and dipole approximations the full Hamiltonian of the problem is written as

$$\hat{H}(x, t) = \frac{1}{2}\left(\hat{p} - \frac{\epsilon_0}{\omega}\sin(\omega t)\right)^2 + \hat{V}(x). \tag{4.1}$$

An inverted Gaussian potential

$$\hat{V}(x) = -V_0 \exp\left[-(x/x_0)^2\right] \tag{4.2}$$

was suggested by Bardsley *et al* [18] for describing the interaction of a Xe electron with an external laser field having a frequency of ω and maximum intensity of $I_0 = (c/8\pi)\epsilon_0^2$ (c is the speed of light in vacuum). For $V_0 = 0.63$ au and $X_0 = 2.65$ au, this potential supports two bound states which mimic the two lowest electronic states of Xe, having energies of $E_0 = -0.4451$ au and $E_1 = -0.1400$ au, and a third weakly bound state with the energy of $E_2 = -0.00014$ au. The frequency ω in equation (4.1) was set to $\omega = 0.0925$ au which is close to a three-photon resonance. The maximum field intensity was varied from 10^{13} W cm^{-2} to 10^{15} W cm^{-2}.

The Hamiltonian (equations (4.1) and (4.2)) was represented on a Fourier grid of between 128 and 512 grid points with a fixed grid step of 0.8 au. Convergence of the results with respect to changes of the grid step and grid size was checked. Different values of the complex rotation angle θ in the range 0.3 to 0.7 were used. Stability of the HG spectrum with respect to changes in (the non-physical parameter) θ was an indication of the accuracy of the results. Time propagation was carried out according to the evolution equation (equation (2.8)) to obtain the quasi-energy resonance states. The resonance state with the largest lifetime was time propagated according to the Schrödinger equation (equation (2.1)). Usually 4096 equal time steps per optical cycle were sufficient to converge the results in both equations (equations (2.8) and (2.1)).

4.2. The study of a non-periodic Hamiltonian

A numerical solution of the time-dependent Schrödinger equation was also performed using a pseudo-spectral representation of the kinetic energy operator with a variable-time-step algorithm for the propagation of the initial state [27]. The grid was chosen to have 4096 points, with a spacing, Δx, of 0.8 a_0. The bound states supported by the potential in equation (4.2) were determined by relaxation in imaginary time using a Chebyshev polynomial expansion of the evolution operator [26]. The energies were found to agree with those which were given by Bardsley *et al* to the accuracy cited. Demanding a step-wise accuracy of 10^{-7} for a fifth-order polynomial expansion ensured that the time-evolution was followed very accurately [27, 28]. It should be noted that the average time-step used by this method was usually a factor of 8–10 smaller than that used in the fixed time-step propagation [18]. That is, $\Delta t_{\text{variable}} \approx 0.07$ au, whereas, $\Delta t_{\text{fixed}} \approx 0.68$ au. Another important difference from earlier calculations is that an absorbing boundary condition was invoked to avoid spurious reflections from the edge of the grid.

The dipole approximation in the radiation gauge was chosen so that the Hamiltonian operator has a similar form to that given in equation (4.1),

$$H(x,t) = \frac{1}{2}\left(p - \frac{e}{c}A(t)\right)^2 + V(x) \tag{4.3}$$

where the vector potential is defined to be

$$A(t) = A_0 \sin^2(\omega t/N)\sin(\omega t) \qquad A_0 = \epsilon_0 c/\omega. \tag{4.4}$$

The parameter N controls the number of optical cycles over which the field is applied and was either chosen to be 50 or 100. The laser field frequency receives the same value as noted above, 0.0925 au. The pulse envelope thus evolves sinusoidally over N optical cycles and vanishes for times greater than that. The harmonic response of the system is calculated by evaluating the time-dependent dipole moment (here we are using the conventional definition of the scalar product)

$$d(t) = \int_{-\infty}^{\infty} \psi^*(x,t)x\psi(x,t)\mathrm{d}x \tag{4.5}$$

and then Fourier transforming this quantity in time

$$\sigma(\Omega) = \left| \int_0^{2\pi N/\omega} \exp^{-\mathrm{i}\Omega t} d(t)\mathrm{d}t \right|^2. \tag{4.6}$$

5. Results and discussion

5.1. The harmonic generation spectrum

The TDCCFM, as described in section 2, was implemented for calculating the resonance quasi-energy states of the inverse Gaussian model Hamiltonian equations (4.1) and (4.2). The results are presented in figure 1(*a*) in the complex λ plane. One can clearly see from this figure the pattern of behaviour which has been previously described. The spiral formed by the continuum is denoted in the picture by open circles, and five quasi-energy

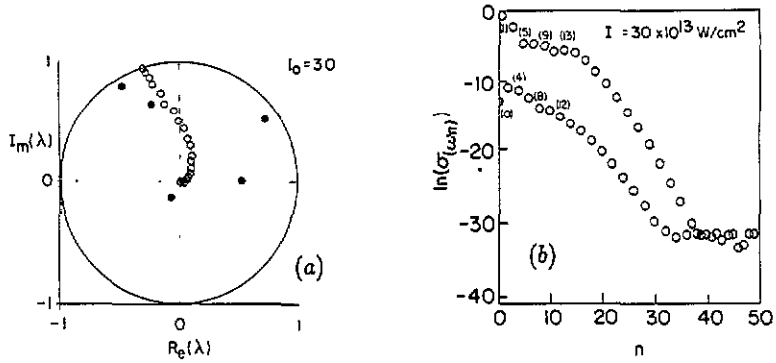

Figure 1. λ_α (*a*) and HG spectrum (*b*) obtained by the largest lifetime resonance state in (*a*) for the model potential given in equations (4) where $\omega = 0.0925$ au, $\theta = 0.5$ rad and $I_0 = 30 \times 10^{13}$ W cm^{-2}.

resonance states, appear outside this spiral and are denoted by full circles. The (non-linear) phenomenon involving the appearance of two 'extra' quasi-energy resonance states on top of the three original bound states of the field-free Hamiltonian was addressed in another study [20]. In this work, we calculated the harmonic generation spectrum, as described in section 3, from the isolated resonance state with the largest lifetime located at the upper right quarter of the unit circle of figure 1(*a*). The results presented in figure 1(*b*) show a typical HG spectrum. The spectrum was found to be insensitive to the value of θ a fact that gives an indication for the quality of the calculation. As a result of symmetry of the potential, even harmonics have lower intensities than the odd ones (an infinite basis set would result in zero peaks for the even harmonics). Looking at the odd harmonics, one can see the familiar behaviour observed in experiments: a sharp exponential decay of the harmonics $\sigma(\omega n)$ from the first to the fifth harmonic (note the logarithmic scale), followed by a plateau between the 5th and the 15th harmonics, and finally the exponential drop from the 15th harmonic onward. This qualitative agreement with experimental observations is not unique to the specific field parameters which were used. A similar pattern of behaviour is shown, for example in figures 3 and 4 for a different choice of field parameters.

5.2. *Correlation of HG and other non-linear phenomena*

In this section, the possible correlation between HG and other non-linear phenomena is examined. The complex λ plane graphically depicts the interaction between different quasi-energy resonance states, and between resonance states and continuum states. The dependence of some of the quasi-energy resonance states on the maximum field intensity I_0 is shown in figure 2. In figure 2(*a*) one can see the behaviour of three resonance states for maximum field intensity in the range $I_0 = 10.5 \times 10^{13}$ W cm^{-2} to 15.5×10^{13} W cm^{-2}. The resonance state that is closest to the contour of the unit circle is correlated to the ground state of the field-free system. For maximum field intensities smaller than $I_0 = 10 \times 10^{13}$ W cm^{-2} (not shown), this resonance state, which has the largest lifetime, is moving counter-clockwise on the unit circle curve with an increase in I_0 [20]. Following this resonance state when the field intensity is increased beyond $I_0 = 10 \times 10^{13}$ W cm^{-2}, one can see that at $I_0 = 12.5 \times 10^{13}$ W cm^{-2}, it goes through an avoided crossing with another resonance state. For intensities greater than $\simeq 13 \times 10^{13}$ W cm^{-2}, this ground state resonance is, again, moving on the unit circle contour as the maximum field intensity is increased (figure 2(*a*)).

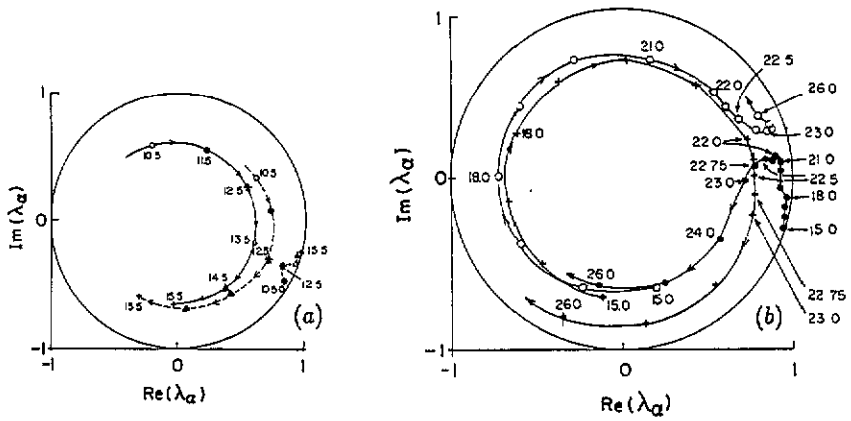

Figure 2. Dependence of λ_α of resonance states in the maximum field intensity, I_0 (in units of 10^{13} W cm^{-2}), for a fixed frequency $\omega = 0.0925$ au. (*a*) I_0 is varied from 10.5 to 15.5 by 1.0 steps. Points that have the same shape mark the same I_0 value. (*b*) I_0 varied from 15.0 to 26.0. Points with the same shape follow the same resonance state.

At even higher intensities (figure 2(*b*)), this resonance state (denoted by full circles) undergoes a pair of successive avoided crossing events (at $I_0 = 22.0 \times 10^{13}$ W cm^{-2} with the resonance state denoted by a plus sign and at $I_0 = 22.5 \times 10^{13}$ W cm^{-2} with the resonance state denoted by an open circle). As a consequence of these two successive avoided crossing events, the ground state resonance makes a 180° turn and starts to move clockwise as the maximum intensity, I_0, is increased. Its lifetime becomes dramatically shorter. Another resonance state (the one denoted by open circles), that prior to the avoided crossing moves clockwise and had a short lifetime makes a 180° turn and starts to move in the opposite direction as I_0 is increased. Its lifetime is drastically increased, such that this state now becomes the resonance state with the largest lifetime and therefore the dominant one with respect to governing the dynamics.

Figures 3 and 4 display the HG spectra behaviour in the vicinity of the two avoided crossing events discussed before. Figure 3 shows the HG spectra for field intensities in the vicinity of the first avoided crossing event near $I_0 = 12.5 \times 10^{13}$ W cm^{-2}. They look very similar to each other. The familiar plateau appearing for high harmonics is clearly seen. A closer look at figure 3(*c*) reveals the fact that the third harmonic for this field intensity ($I_0 = 12.5 \times 10^{13}$ W cm^{-2}) is higher than the third harmonic in the other pictures for which I_0 is either higher (3(*d*), 3(*e*)) or lower (3(*a*), 3(*b*)) than 12.5×10^{13} W cm^{-2}. Figure 4 shows the same phenomenon for field intensities in the surrounding of the second avoided crossing event at $I_0 \simeq 22.5 \times 10^{13}$ W cm^{-2}. The third harmonic for $I_0 = 22.5 \times 10^{13}$ W cm^{-2} (figure 4(*b*)) is relatively higher than the third harmonic for both lower (figure 4(*a*)) and higher (figure 4(*c*)) maximum field intensities. Those results suggest a possible correlation between HG and the occurrence of avoided crossing events.

The numerical observation that during the two avoided crossing events the intensity of the third harmonic is amplified raises a question as to the reason for the amplification of this specific harmonic. This question is out of the scope of this paper and is left to further work, which is currently underway. Some directions which are being investigated are the following.

(i) An avoided crossing between two resonance states, causes some mixing between them [30]. It might be the case that the two avoided crossings events discussed above

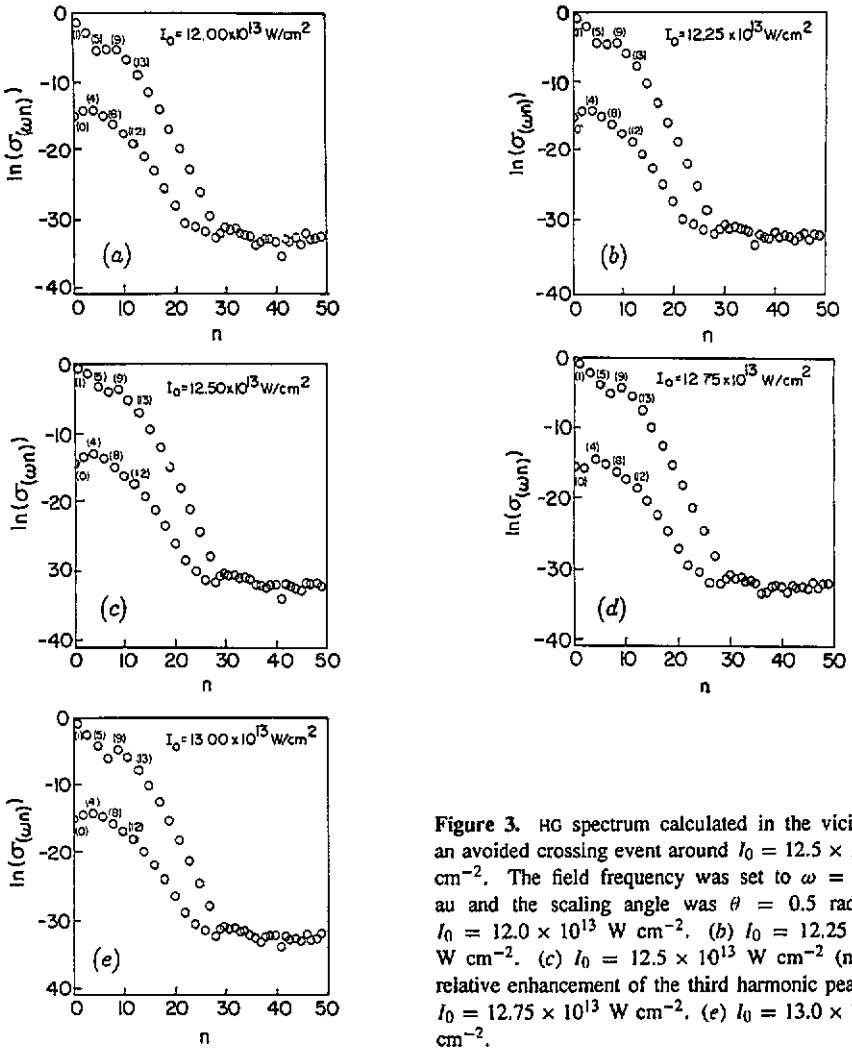

Figure 3. HG spectrum calculated in the vicinity of an avoided crossing event around $I_0 = 12.5 \times 10^{13}$ W cm^{-2}. The field frequency was set to $\omega = 0.0925$ au and the scaling angle was $\theta = 0.5$ rad. (*a*) $I_0 = 12.0 \times 10^{13}$ W cm^{-2}. (*b*) $I_0 = 12.25 \times 10^{13}$ W cm^{-2}. (*c*) $I_0 = 12.5 \times 10^{13}$ W cm^{-2} (note the relative enhancement of the third harmonic peak). (*d*) $I_0 = 12.75 \times 10^{13}$ W cm^{-2}. (*e*) $I_0 = 13.0 \times 10^{13}$ W cm^{-2}.

consisted (by chance) of an interaction between the ground state resonance and a resonance state which is associated with the third bound state. As a consequence it was the third harmonic that was enhanced.

(ii) The third harmonic amplification might be due to the fact that the field frequency was set close to a three-photon resonance.

If both explanations (i) or (ii) are correct, they provide a possible mechanism for obtaining an amplification of a single high harmonic as is needed for creating an efficient coherent x-ray source. According to explanation (i), a search for an avoided crossing of the ground state resonance (of a hypothetical system) with some *high* resonance state might prove helpful. According to explanation (ii), the solution might be to search for an avoided crossing of the ground state resonance with the field frequency set near a many-photon resonance.

5.3. Very strong fields—spectrum inversion

As the field intensity, I_0, is increased, our method of interpreting the exact results, which

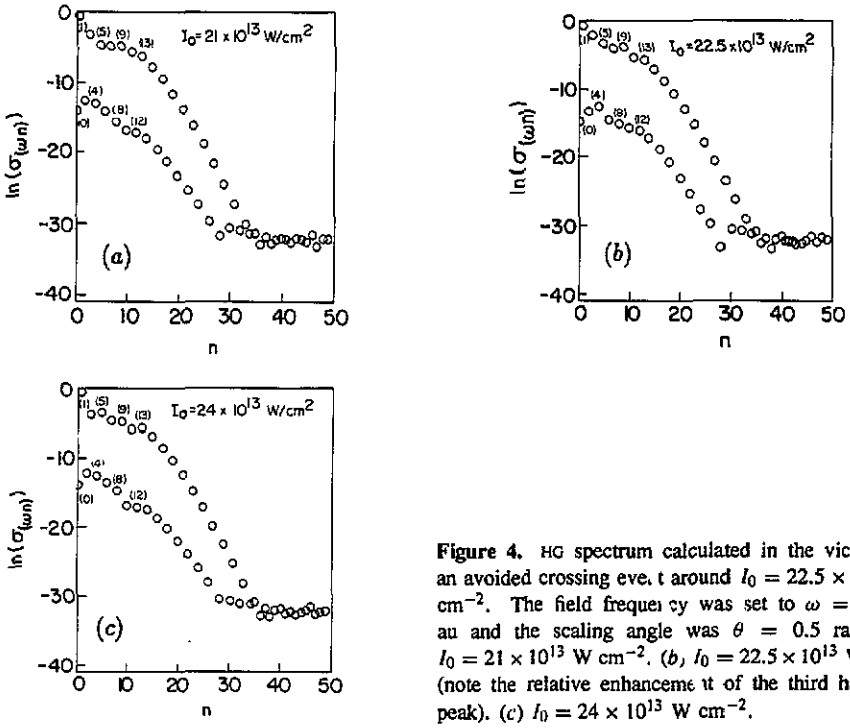

Figure 4. HG spectrum calculated in the vicinity of an avoided crossing event around $I_0 = 22.5 \times 10^{13}$ W cm^{-2}. The field frequency was set to $\omega = 0.0925$ au and the scaling angle was $\theta = 0.5$ rad. (*a*) $I_0 = 21 \times 10^{13}$ W cm^{-2}. (*b*) $I_0 = 22.5 \times 10^{13}$ W cm^{-2} (note the relative enhancement of the third harmonic peak). (*c*) $I_0 = 24 \times 10^{13}$ W cm^{-2}.

was based on a perturbative concept of the system, breaks down. Not only does it become more and more difficult to map the resonance states onto the field free bound states, but, as is clearly seen in figures 1(*a*), 5(*a*) and 6(*a*), more resonance states appear [20]. Terms like 'the ground state resonance' lose their meaning. As I_0 is increased, the system undergoes more and more avoided crossing events and the information about the identity of a specific state is lost.

The HG spectrum calculated by analysis of the narrowest (largest lifetime) resonance for the very high field intensity of $I_0 = 50 \times 10^{13}$ W cm^{-2} is shown on a logarithmic scale in figure 5(*c*) and on a non-logarithmic scale in figure 5(*b*). For such high field intensities, it happened that the third harmonic was the most probable one.

For most of this work we calculated the harmonic generation spectrum under the assumption that the dynamics of the system, including harmonic generation, is governed at each field intensity solely by the largest lifetime resonance at that intensity. We would like now to find out whether the consideration of additional shorter-lifetime resonances has any observation on the major effect indicated by our calculations which is the appearance of very intense high harmonics at high field intensities the ('inverted' spectrum which is shown in figure 5(*b*)). In figure 6(*a*), one can see the five resonance states presented in the complex λ plane for maximum field intensity of $I_0 = 60 \times 10^{13}$ W cm^{-2}. The HG spectrum presented in figure 6(*b*) (non-logarithmic scale), and figure 6(*c*) (logarithmic scale) was calculated from the resonance state with the *second largest lifetime* ($\lambda_\alpha \simeq 0.37 + i0.62$). In those figures, we see that the fifth harmonic has the highest intensity. From figure 6 we conclude that even in cases where more than one resonance state is required for an adequate description of the physical system, still the highest intensity peak in the HG spectrum is not necessarily the driving frequency, and one may obtain an 'inverted' spectrum. Note that the contribution from the two states (or however many states are used) should have been

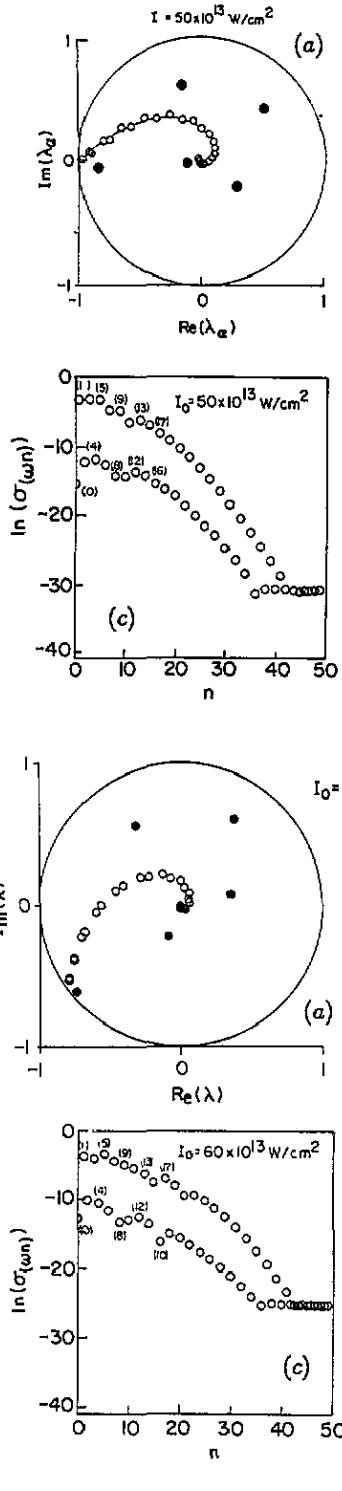

Figure 5. λ_α (*a*) and HG spectrum in a non-logarithmic scale (*b*) and logarithmic scale (*c*) obtained by the largest lifetime resonance state in (*a*) for the model potential given in equations (4) where $\omega = 0.0925$ au $\theta = 0.5$ rad and $I_0 = 50 \times 10^{13}$ W cm^{-2}.

Figure 6. λ_α (*a*) and HG spectrum in a non-logarithmic scale (*b*) and logarithmic scale (*c*) obtained by the second largest lifetime resonance state in (*a*) for the model potential given in equations (4) where $\omega = 0.0925$ au $\theta = 0.5$ rad and $I_0 = 60 \times 10^{13}$ W cm^{-2}.

added coherently. Therefore, the results presented in figure 6 give only a rough estimation of the error caused by the assumption that a single state determines the dynamics which we have made throughout this work.

The qualitative agreement between results of our model calculations for high field intensities (up to $I_0 \sim 30 \times 10^{13}$ W cm^{-2}) and experimental results consolidates our belief in the ability of the methods developed here to accurately analyse the behaviour of physical systems in high laser fields. Since the TDCCFM is a non-perturbative method, we see no reason for the validity of its use to break down at even higher field intensities. We therefore expect the numerical prediction of obtaining a HG spectrum having the highest intensity peak at a frequency other than the driving frequency, to be confirmed by experiment.

5.4. Effects caused by the non-periodicity of the Hamiltonian

At this point it is worthwhile to consider the issue of relating the Floquet analysis which is basically a CW approach, to the short pulse experiments [1, 2] which are required to obtain the high field intensity. Two extreme situations can be encountered depending on the rate of the turn on of the pulse. In the sudden limit the pulse will create a superposition of resonances and continuum states. Due to the high kinetic energy acquired by the electrons, they leave the interaction region quickly and are not trapped by the pondermotive potential. This means that after a short induction period the longest living resonance will dominate the dynamics. The other extreme is a pulse with an adiabatic turn on. In this case the system will stay on the resonance correlated with the ground state. One can conclude that at least up to the field intensity where the first avoided crossing event occurs, the ground state resonance has the longest lifetime and the sudden and adiabatic pulses will lead essentially to similar results. This result has been confirmed by comparing the HG calculated by the TDCCFM method to a direct solution of the time dependent Schrödinger equation incorporating the pulse shape (equation (4.3)). For field intensities above the intensities where avoided crossing events occur, the shape of the turn on function will determine whether the system will follow the adiabatic curve or whether it will mix with other resonances and again be dominated by the resonance with longest lifetime.

In order to be able to evaluate the influence of the pulse envelope on the HG spectra, we present HG spectra which were obtained by solving the time-dependent Schrödinger equation with the non-periodic Hamiltonian given in equations (4.1)–(4.3) which includes the temporal envelope.

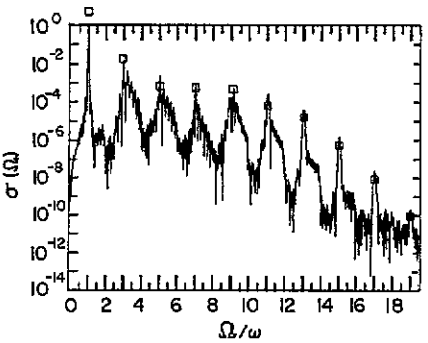

Figure 7. HG spectrum, equations (4.5)–(4.6), obtained by a direct solution of the time-dependent Schrödinger equation with the non-periodic Hamiltonian which is given in equations (4.3)–(4.4) with $\omega = 0.0925$ au, $I_0 = 21 \times 10^{13}$ W cm^{-2} and $N = 100$. The results of the TDCCFM (same as figure 4(*a*)) are denoted by squares. Those results have been multiplied by a constant factor so as to obtain a fit for the 9th harmonic peak.

The amplitude of the Fourier transformed dipole moment is plotted in figure 7 as a function of energy in unit of the applied field frequency, ω, to emphasize the spectral features at integral photon emission. The number of optical cycles, N, was 100 and the intensity was 21×10^{13} W cm^{-2}. The plotted amplitudes are scaled to the value of the largest peak emission which in this case is at one photon unit, 0.0925 Hartree. There is a large amount of sub-harmonic structure in the calculated emission, especially to the higher energy side of each odd harmonic. This typical figure manifests a similar pattern of behaviour as the one observed in experiments: the exponential drop, from the 1st to the 5th harmonics, is followed by a plateau, between the 5th and the 9th harmonics, and then ends with a final drop from the 9th harmonic onwards. HG spectra which were obtained by the TDCCFM (assuming a periodic Hamiltonian) are denoted by squares in the figure. Note that the results of both calculations were superimposed, and that the TDCCFM values were multiplied by a constant factor as to obtain a fit for the 9th harmonic peak. Comparing the HG spectra, one observes only minor deviations. An overall agreement with minor deviations was found also for other field intensity parameters and even for the narrower pulses ($N = 50$).

One might attempt to draw a connection between two characteristic times: the period of the external field, T, and the lifetime of the quasi-emergy resonance state, τ_{res} and argue that the Floquet ansatz is applicable only for resonance states with lifetimes significantly larger than few optical cycles. There is no basis for such a limitation. The floquet ansatz depends only on the pulse envelope. For an inherently periodic system, the Floquet theorem suggests the existence of periodic solutions to the Schrödinger equation (2.1) regardless of their lifetimes.

Table 1. The ratio between lifetimes of quasi-energy resonance states, τ_{res} and the period of the field, T, for different field intensities, I_0, for a constant frequency, $\omega = 0.0925$ au. The results are calculated for the resonance state with the longest lifetime except for case IV where the resonance with the second longest lifetime is considered.

	I_0 (10^{13} W cm^{-2})	τ_{res}/T	Figure number
I	21	~ 7	2(*b*)
II	30	~ 8	1(*a*)
III	50	~ 7	5(*b*)
IV	60	> 1	6(*a*)

In table 1 we show the ratio τ_{res}/T for various field intensities I_0 for a fixed frequency $\omega = 0.0925$ au. Note that for $I_0 = 21 \times 10^{13}$ W cm^{-2} there was an agreement between the results obtained by the Floquet calculations and the direct solution of the Schrödinger equation incorporating a pulse envelope. The agreement for $\tau_{res}/T \simeq 7$ is a numerical example of the fact that the Floquet theory is applicable regardless of the lifetime of the resonance of the quasi-energy state.

The pulses used in this work ($N = 50$ or 100 in equation (4.3)) are even shorter than the pulses reported to be used in experiments [(1, 2)] ($N > 300$). Therefore, the agreement between the results obtained by the two approaches indicates that the Floquet analysis is reliable despite the lack of consideration of the pulse envelope.

6. Concluding remarks

The time-dependent complex coordinate Floquet method (TDCCFM) which is a non-perturbative accurate method adequate for the description of systems under the influence of

intense external fields was presented in this work. The major advantage of this method is its ability to describe the whole dynamics by a single, L^2, square integrable wavefunction, amenable to the application of bound state techniques. We have shown that the TDCCFM accompanied by the representation of the quasi-energy resonance states in the complex λ plane, provides an accurate and easy to use method for the investigation of various non-linear phenomena which occur when placing an atom or a molecule in an external intense laser field. These phenomena include an avoided crossing, appearance and disappearance of the quasi-energy resonance states as a function of changing the maximum field amplitude or frequency, harmonic generation and above threshold ionization/dissociation (ATI/D). The correlation between ATI and HG has already been pointed out by Eberly *et al* [12]. In this study we numerically demonstrated the correlation between HG and other non-linear phenomena which were listed above.

In view of the connection between the HG and ATI phenomena it is interesting to mention that although an inverted ATI spectrum (i.e. suppression of the 'slow' electron peak relative to the fast electron peaks) has been observed both experimentally [31] and theoretically [32, 33], an 'inversion' in HG spectra has never been observed either experimentally or theoretically. In this work we numerically observed such an 'inversion' for the first time.

The backbone assumption of the TDCCFM is the periodicity of the Hamiltonian. This assumption is in contradiction with the pulse laser sources which are used in experiments. Nevertheless, the results obtained by the TDCCFM are in agreement with results obtained by a direct solution of the time-dependent Schrödinger equation incorporating a pulse envelope which is even narrower than the pulse envelopes which are used in experiments.

In the present work we used a short-range potential (equation (4.2)), but we have successfully applied the time-dependent complex coordinate Floquet theory to the long-range 'soft' Coulomb potential:

$$V = -\left(1 + x^2\right)^{-1/2} \tag{6.1}$$

suggested by Su and Eberly [34]. As is the case for atomic systems, this potential has a Rydberg series converging to the continuum. It was found that the long range behaviour of the semi-Coulomb potential does not cause any additional difficulty relative to short range potentials. This numerical observation may be explained by the use of the complex coordinate method which provides absorbing boundary conditions that cause localization of the resonance quasi-energy wavefunction.

Calculating the HG spectrum through the TDCCFM, although very compact, results in an oversimplified spectrum (i.e. no sub-harmonics and no widths). This is due to the neglect of interactions between different resonance states and between resonance and continuum states.

This paper concentrated on the interaction of a system with a single external field. A different strategy for amplification of high harmonics in the HG spectrum might arise from the simultaneous use of several radiating fields to suppress all of the low-order multiples of the irradiating frequency of the strongest field such that only a single very high harmonic will still exist. The dressed picture formalism or the theory of optimal control [35] may provide guidelines for the proper choice of field parameters for such spectra to be obtained.

We have made no attempt at obtaining *quantitative* agreement between our model results and HG spectra obtained by experiments in rare-gas atoms exposed to high external laser fields. The model potential used is only a crude approximation to a Xe atom in a laser field. Nevertheless, the spectra obtained by this model are in *qualitative* agreement with experimental observations. In light of this qualitative agreement, we expect experimental

verification to the prediction that atoms which are exposed to very strong laser fields, will show an inverted HG spectrum, having the highest intensity for harmonics other than the driving frequency. In order to measure such phenomena, it is necessary to distinguish between photons coming from the irradiated sample and photons which come directly from the radiating laser. This might be impossible. It might be possible to observe a similar experimental situation where some harmonic higher than the third has intensity higher than the intensity of the third harmonic. Such experiments may mark a stage toward the desired goal of reaching an efficient coherent x-ray source through high harmonic generation.

Acknowledgments

This work was supported in part by the Basic Research Foundation administrated by the Israeli Academy of Sciences and Humanities, and by the S and N Grant Research Fund, by the Technion VPR Fund–Smoler Research Fund, and by the Fund for the Promotion of Research at the Technion. Research at Lawrence Livermore National Laboratory is performed under the auspices of the US Department of Energy under Contract No W-7405-ENG-48. We would like to thank Dr N Lipkin for useful discussions and comments and Professor Eberly for his suggestion to apply our method to the long-range 'soft' Coulomb potential.

References

[1] Ferray M, L'Huillier A, Li X F, Lompré L A, Mainfray G and Manus C 1988 *J. Phys. B: At. Mol. Opt. Phys.* **21** L31
[2] Li X F, L'Huillier A, Ferray M, Lompré L A and Mainfray G 1989 *Phys. Rev.* A **39** 5751
[3] Kaminski J Z 1990 *Phys. Lett.* **151A** 308
[4] L'Huillier A, Schafer K J and Kulander K C 1991 *Phys. Rev. Lett.* **66** 2200
[5] L'Huillier A, Schafer K J and Kulander K C 1991 *J. Phys. B: At. Mol. Opt. Phys.* **24** 3315
[6] Rosen M D *et al* 1985 *Phys. Rev. Lett.* **54** 106
Matthews D L *et al* 1985 *Phys. Rev. Lett.* **54** 110
Key M H 1985 *Nature* **316** 314
[7] Matthews D L and Rosen M D 1988 *Sci. Am.* December 58
[8] Leopold J G and Richards D 1993 *J. Phys. B: At. Mol. Opt. Phys.* submitted
Bandarage G, Maquet A and Cooper J 1990 *Phys. Rev.* A **41** 1744
[9] Kulander K C and Shore B W 1989 *Phys. Rev. Lett.* **62** 524; 1990 *J. Opt. Soc. Am.* B **7** 502
Kulander K C, Schafer K J and Krause J L 1993 *Int. J. Quantum Chem.* in press
[10] Becker W, Long S and McIver J K 1990 *Phys. Rev.* A **41** 4112
Brunel F 1990 *J. Opt. Soc. Am.* B **7** 521
[11] Sundaram B and Milonni P W 1990 *Phys. Rev.* A **41** 6571
[12] Eberly J H, Su Q and Javanainen J 1989 *Phys. Rev. Lett.* **62** 881; 1989 *J. Opt. Soc. Am.* B **6** 1290
[13] Potvliege R M and Shakeshaft R 1989 *Phys. Rev.* A **40** 3061
[14] DeVries P L 1990 *Opt J. Soc. Am.* B **7** 517
[15] Szöke A 1988 *Atomic and Molecular Processes with Short Intense Laser Pulses* ed Andre B Bandrauk (New York: Plenum); 1992 Private communication
[16] Kulander K C 1987 *Phys. Rev.* A **35** 445
[17] Pan L, Taylor K T and Clark C W 1990 *J. Opt. Soc. Am.* B **7** 509
[18] Bardsley J N, Sz Aöke and Comella M J 1988 *J. Phys. B: At. Mol. Opt. Phys.* **21** 3899
[19] Ben-Tal N, Moiseyev N, Leforestier C and Kosloff R 1991 *J. Chem. Phys.* **94** 7311
[20] Ben-Tal N, Moiseyev N and Kosloff R 1993 *J. Chem. Phys.* submitted
[21] Floquet M G 1983 *Ann. Ec. Norm. Suppl.* **12** 47
Shirley J H 1965 *Phys. Rev.* **138** B979
Maquet A, Chu S-I and Reinhardt W P 1983 *Phys. Rev.* A **27** 2946

Chu S-I 1985 *Adv. At. Mol. Phys.* **21** 197
Manakov N L, Ovsiannikov V D and Rapport L P 1986 *Phys. Rev.* **141** 319
Potvliege R M and Shakeshaft R 1988 *Phys. Rev.* A **38** 4597; 1989 *Phys. Rev.* A **39** 1545
[22] Balslev E and Combes J M 1971 *Commun. Math. Phys.* **22** 280
[23] Junker B R 1982 *Adv. At. Mol. Phys.* **18** 207
Reinhardt W P 1983 *Ann. Rev. Phys. Chem.* **33** 223
Ho Y K 1983 *Phys. Rep.* **99** 1
[24] Sakurai J J 1985 *Modern Quantum Mechanics* (New York: Addison-Wesley) ch 2
[25] Kosloff R 1988 *J. Phys. Chem.* **92** 2087
[26] Leforestier C *et al* 1991 *J. Comput. Phys.* **94** 59
[27] Ezer H T, Kosloff R and Cerjan C 1992 *J. Comput. Phys.* **100** 179
[28] Cerjan C and Kosloff R 1992 *Phys. Rev.* A submitted
[29] Moiseyev N, Certain P R and Weinhold F 1978 *Mol. Phys.* **36** 1613
Moiseyev N 1989 *Lecture Notes in Physics* **324** ed E Brandas and N Elander (Berlin: Springer) p 459; 1991 *Isr. J. Chem.***31** 311
[30] Moiseyev N and Korsch J 1990 *Isr. J. Chem.* **30** 107
[31] Agostini P, Kupersztych J, Lompre L A, Petite G and Vergeau F 1987 *Phys. Rev.* A **36** 4111
Freeman R R, McIlrath T J, Bucksbaum P H and Bashkansky M 1986 *Phys. Rev. Lett.* **57** 3156
[32] Moiseyev N, Bensch F and Korsch H J 1990 *Phys. Rev.* A **42** 4045
Bensch F, Korsch H J and Moiseyev N 1991 *Phys. Rev.* A **43** 5145
[33] Eberly J H and Javanainen J 1988 *Eur. J. Phys.* **9** 265
[34] Su Q and Eberly J H 1991 *Phys. Rev.* A **44** 5997
[35] Kosloff R, Rice S A, Gaspard P, Tersigni S and Tannor D 1989 *Chem. Phys.* **139** 201
Shi S, Woody A and Rabitz H 1988 *J. Chem. Phys.* **88** 6870